ADVANCES IN ATMOSPHERIC SCIENCES, VOL. 23, NO. 6, 2006, 1003–1019

Interannual Thermocline Signals and El Niño-La Niña Turnabout in the Tropical Pacific Ocean

QIAN Weihong*[1] (钱维宏) and HU Haoran[2] (胡豪然)

[1] *Monsoon and Environment Research Group, School of Physics, Peking University, Beijing* 100871

[2] *Institute of Plateau Meteorology, CMA, Chengdu* 610071

(Received 19 April 2006; revised 23 June 2006)

ABSTRACT

One of the fundamental questions concerning the nature and prediction of the oceanic states in the equatorial eastern Pacific is how the turnabout from a cold water state (La Niña) to a warm water state (El Niño) takes place, and vice versa. Recent studies show that this turnabout is directly linked to the interannual thermocline variations in the tropical Pacific Ocean basin. An index, as an indicator and precursor to describe interannual thermocline variations and the turnabout of oceanic states in our previous paper (Qian and Hu, 2005), is also used in this study. The index, which shows the maximum subsurface temperature anomaly (MSTA), is derived from the monthly 21-year (1980–2000) expendable XBT dataset in the present study. Results show that the MSTA can be used as a precursor for the occurrences of El Niño (or La Niña) events. The subsequent analyses of the MSTA propagations in the tropical Pacific suggest a one-year potential predictability for El Niño and La Niña events by identifying ocean temperature anomalies in the thermocline of the western Pacific Ocean. It also suggests that a closed route cycle with the strongest signal propagation is identified only in the tropical North Pacific Ocean. A positive (or negative) MSTA signal may travel from the western equatorial Pacific to the eastern equatorial Pacific with the strongest signal along the equator. This signal turns northward along the tropical eastern boundary of the basin and then moves westward along the north side of off-equator around 16°N. Finally, the signal returns toward the equator along the western boundary of the basin. The turnabout time from an El Niño event to a La Niña event in the eastern equatorial Pacific depends critically on the speed of the signal traveling along the closed route, and it usually needs about 4 years. This finding may help to predict the occurrence of the El Niño or La Niña event at least one year in advance.

Key words: El Niño event, thermocline variation, early signal, tropical Pacific

doi: 10.1007/s00376-006-1003-4

1. Introduction

One of the fundamental questions concerning the nature and prediction of the oceanic states in the eastern equatorial Pacific is how the turnabout from a cold state (La Niña) to a warm state (El Niño) takes place, and vice versa. Recent studies show that this turnabout is directly linked to the interannual variations of the thermocline in the tropical Pacific basin (Li, 1997; Li and Mu, 1999; Chao et al., 2002; Li, 2002). The turnabout from El Niño to La Niña and vice versa in the equatorial eastern Pacific is known as an irregular low-frequency oscillation characterized by the reappearance of the warm and cold sea surface temperature anomalies (SSTA) on the interannual timescale.

Thermocline depth variations are considered to play a key role in the evolution of warm-cold waters in the tropical Pacific Ocean (Qian et al., 2004). It has been considered that the thermocline variations "memorize" the change in the surface wind and provide a delayed feedback, which may be critical in turning the coupled ocean-atmosphere system from a warm state to a cold one or vice versa (Zebiak and Cane, 1987). Wind stress forcing via Ekman pumping and the propagation of the Rossby and Kelvin waves are two processes to lead to the thermocline variations in the tropical Pacific Ocean (Boulanger and Menkes, 1995; Yang et al., 1997).

To represent thermocline variations, several indices have been proposed in the previous investigations. Meyers (1979) studied the annual variation of the thermocline represented by the 14°C isotherm depth de-

*E-mail: qianwh@pku.edu.cn

termined from expendable bathythermograph (XBT) data. He found annual Rossby waves propagating westward along 6°N in the central and western Pacific. Kessler (1990) defined the depth of the 20°C isotherm to represent thermocline depth variations. He found that the depth anomalies of the 20°C isotherm propagated westward across the basin as a long Rossby wave near 5°N and 14°–18°N, while the annual cycle around 10°N is dominated by local Ekman pumping.

Wang et al. (2000) and Chao et al. (2002) pointed out the shortcomings of these two indices in illustrating the thermocline variations. The sea surface temperature in the southern part of the eastern Pacific is less than 20°C in the cold-water period (Qian et al., 2004). On the other hand, the 14°C isotherm is much too deep to represent the thermocline temperature in the warm pool. Wang et al. (2000) defined an index, the location-dependent representative T_c, as characterizing the temperature in the center of the thermocline layer. The representative temperature T_c is defined by averaging the value 12°C (at the base of the thermocline layer) and the long-term mean sea surface temperature locally. Under this definition, the signal of the depth anomalies propagates eastward along the equator only in the region of 2°S–2°N and westward in the off-equatorial wave guides along 5°N (3°–7°N) and 6°S (3°–9°S) to the western boundary. A curved surface (climatological depth) of maximum sea temperature anomalies was proposed by Chao et al. (2002) and the temperature anomalies on the curved surface were used to indicate the thermocline variations. They found that the subsurface temperature anomalies on the curved surface traveled along two closed routes in the tropical off-equator ocean. The signal propagates eastward along the equator and westward along both 10°N and 10°S.

For the first three definitions, the indices are directly involved in the variations of the thermocline depth with respect to the specific temperatures (14°C, 20°C, and T_c). For the latter definition, the index is the temperature anomaly at a specific depth rather than the monthly maximum temperature anomaly at a vertical profile. By comparing with the three definitions, Yu and Qiao (2003) analyzed the positive heat content anomalies (HCA) of the 400-meter upper-layer ocean which represent the warm signals for El Niño events in the interannual timescale. The HCA may include temperature anomaly signals from both the surface and the subsurface layers.

The observed representative temperature at the central depth of the thermocline, or the largest vertical temperature gradient, varies with location (depth) and time. Therefore, a better index to represent the thermocline variations should be a function of depth and time, i.e., neither specific depth nor specific temperature can be decided first. In this paper, we will not investigate the causes that lead to the thermocline variations. The goal of this paper is to further discuss the importance of our previous index for the thermocline variation in the tropical Pacific (Qian and Hu, 2005) and to answer the question of where the thermocline variation in the equatorial eastern Pacific comes from and where it goes to. In the next section, we will examine whether the MSTA can be used as an indicator of thermocline variations in the tropical Pacific, and to see how the MSTA is associated with the development of El Niño through a composite analysis with four El Niño events. Plots for signal propagations along and off the equator as well as other diagrams to display the vertical structure of the MSTA in the tropical Pacific Ocean are shown in section 3. A comparison of the MSTA and the HCA indicating the El Niño turnabout is illustrated in section 4. Finally, conclusions and discussions are given in section 5.

2. Data and index of thermocline variation

2.1 *Data and method*

In order to analyze structures of the upper oceanic temperature field and the propagation features of thermocline signals, the monthly surface-subsurface temperature data (White, 1995) provided by the Joint Environmental Data Analysis Center at the Scripps Institution of Oceanography in the period from January 1955 till December 2000 (5-degree longitude by 2-degree latitude) is used in this study. For this data, the standard depths are 0, 20, 40, 60, 80, 120, 160, 200, 240, 300, and 400 m, respectively. The dataset uses all available thermal observations throughout the worldwide basin, including sea surface temperature (SST)

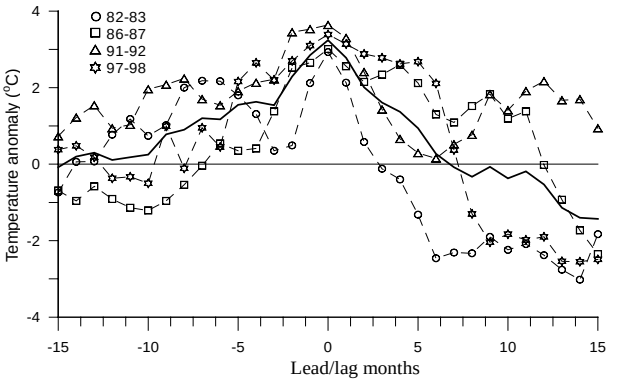

Fig. 1. Time series of MSTA (°C) in the Niño-3 region for four cases and their composite from the leading month–15 to the lagging month+15. The months of maximum MSTA in the Niño-3 region are March 1983, December 1986, March 1992, and September 1997, respectively.

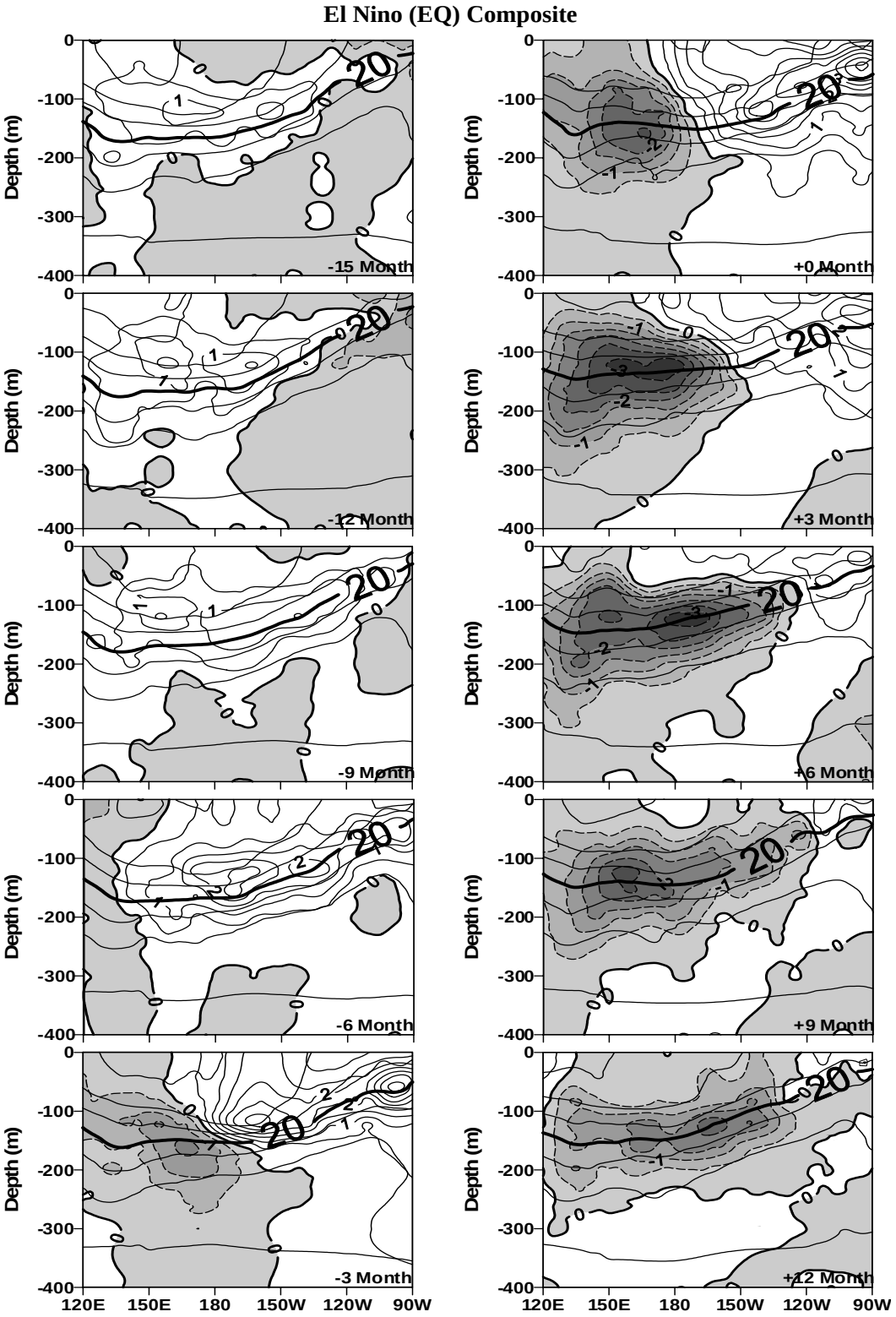

Fig. 2. Depth-longitude diagrams of subsurface temperature (°C, solid line) and their anomalies (°C, light solid and dashed lines) along the equator from different leading and lagging months relative to the month of the largest MSTA for composite El Niño. The shaded are negative. The contour intervals are 3°C for subsurface temperature and 1°C for their anomalies, respectively. The 20°C isotherm is highlighted.

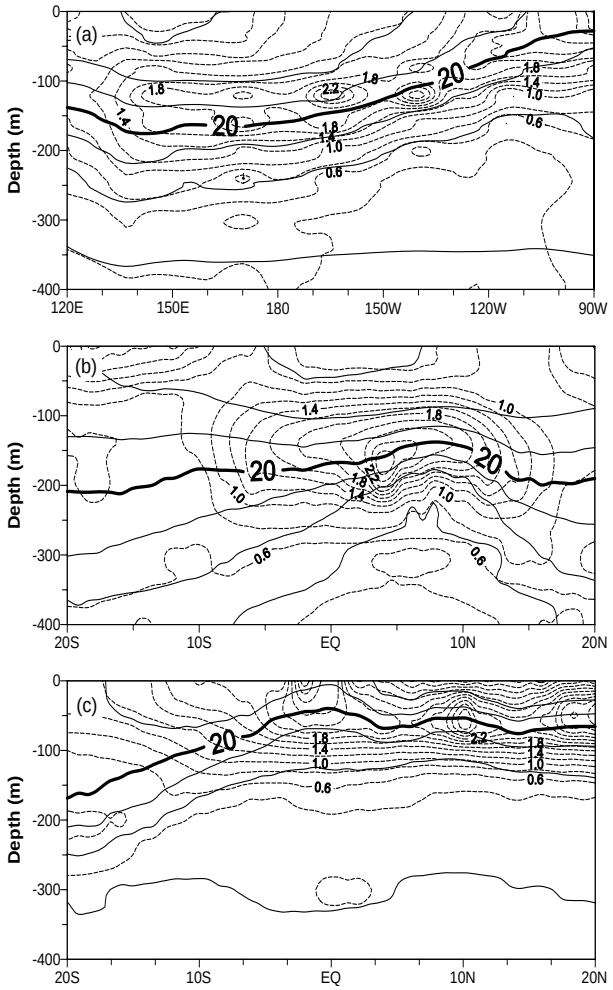

Fig. 3. Standard deviations (dashed lines) based on monthly mean subsurface temperature anomalies (°C) and climatological mean isotherms (6°C, solid lines) along the equatorial Pacific, 150°E, and 100°W sectional diagrams. The contour interval is 3°C for temperature, with the 20°C isotherm highlighted.

measured from ships and buoys, and subsurface temperature measured from XBTs and moored buoys. Data are available mainly in the tropical Pacific and the North Pacific, however there are few measurements in the south of 20°S in the Pacific. Thus, the data in the region of 20°S to 30°N and 110°E to 90°W are analyzed only. Due to the fact that an interdecadal transition of SST occurs in the middle of the 1970s and El Niño features are different after 1980 (Wang, 1995; Qian et al., 1999) in comparison to those before 1980 (Rasmusson and Carpenter, 1982), the data used in this paper are from January 1980 to December 2000 only. Annual means are removed from the original data, thus interannual components are stood out from the variations. Standard deviation as well as leading, concurrent, and lagging correlations are calculated to reveal their characteristics and the connection between the SSTA and the MSTA. A composite analysis is also conducted to show the common features in the El Niño turnabout period.

2.2 *Thermocline Variation*

It is expected that an ideal index for the thermocline variations should be able to record the oceanic energy storage and to memorize the wind forcing, or at least be able to indicate an anomalously strong signal in the upper ocean. In our recent work (Qian et al., 2003, 2004), an indicator—MSTA—is defined to represent the thermocline variations through the case's analyses in the tropical Pacific Ocean and the tropical Indian Ocean. In the tropical Indian Ocean, a dipole structure of MSTA in the subsurface ocean is revealed (Qian et al., 2003). To examine the common characteristics, four El Niño events (1982/83, 1986/87, 1991/92, and 1997/98) are used for a composite analysis. The El Niño events are defined by the months when the maximum positive MSTA appeared in the Ninõ-3 region (5°N–5°S, 150°–90°W). The time is identified to be March 1983, December 1986, March 1992, and September 1997, respectively.

Figure 1 shows the time series of the MSTA in the Niño-3 region for the four El Niño events and their composite during the period of the month−15 (The MSTA in the Niño-3 leads) to the month+15 (The MSTA in the Niño-3 lags). A smooth evolution can be observed in the composite time series with the positive MSTA from the month−14 to the month+6 and the negative MSTA after the month+7. A +3°C anomaly value is found in the month 0 and a −1.5°C anomaly center appears after the month+12, but the amplitude is relatively larger after the month+5. The composite time series matches well with the evolution process of the El Niño, with the onset speed faster than the withdrawal speed.

To examine the composite subsurface temperature anomaly (STA), Fig. 2 displays the depth-longitude diagrams of subsurface temperature and its anomaly along the equator from different leading and lagging months relative to the month of the maximum MSTA in the Niño-3 region. In the month−15 relative to the largest MSTA in the Niño-3 region, a major positive core of STA appears in the equatorial western Pacific close to the depth of 110 m. The 20°C isotherm is below the core. The positive core gradually extends eastward from the monthe−15 to the month−9 and is always above the 20°C isotherm, but the negative STA retreats eastward and toward the surface in the equatorial eastern Pacific. In the month−9, positive subsurface temperature anomalies control the entire equatorial basin with a core in the central Pacific. From the month−6 to the month−3, positive subsurface temper-

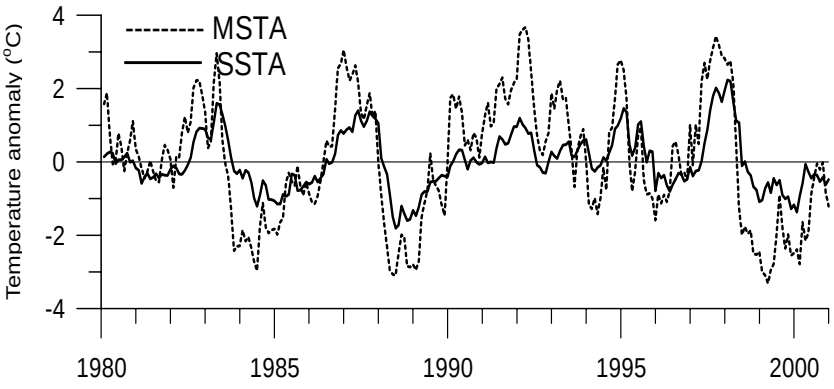

Fig. 4. Time series of SSTA (°C) and MSTA (°C) in the Niño-3 region (5°N–5°S, 150°–90°W) from 1980 to 2000.

ature anomalies are strengthened and move eastward along the 20°C isotherm in the equatorial central Pacific. In the mature month of the composite El Niño event, a positive core with the value 3°C is located in the equatorial eastern Pacific at the depth of 50 m while a negative core with the value −3°C is located in the equatorial western Pacific at the depth of 160 m. A dipole structure in the subsurface temperature anomalies can be obviously noted in the mature phase of the El Niño. After then, the positive subsurface temperature anomalies are weakened in the equatorial eastern Pacific, meanwhile the negative subsurface temperature anomalies are strengthened in the west and move eastward along the 20°C isotherm. From the month+3 to the month+9, a positive temperature anomaly remains near to the surface, however a negative temperature anomaly already occupies over the subsurface in the central Pacific.

The climatological features of the subsurface temperature anomalies in the zonal-vertical profile at the equator and the meridional-vertical profiles at 150°E and 100°W can be noted in Fig. 3. In the zonal-vertical profile at the equator, the depth of the 20°C isotherm indicates the climatic mean position of the thermocline in 1980–2000. The standard deviation (SD) based on monthly mean ocean temperature anomalies shows thermocline variations in this period. In the central Pacific (130°–170°W), two large SD centers with values about 2.4°C are located at the depth of 110 m. In the equatorial eastern Pacific (90°W), the maximum SD center (2.8°C) is near the surface. In contrast with those in the central-eastern Pacific, a lower SD with a value about 0.6°C is situated in the equatorial western Pacific and near to the surface. In the western and central Pacific, the maximum SD axis is located above the 20°C isotherm, while its counterpart in the eastern Pacific is located just along the 20°C isotherm.

The thermocline in the warm pool actually shows the strong variability only in the region between 10°S and 20°N (Fig. 3b). To the south of 10°S, the weak variability in the thermocline can be noted as well. The maximum SD (2.6°C) in the meridional-vertical profile at 150°E is located near 4oN and at the depth of 160 m. Another large SD (1.4°C) is near to the surface in the south of 10°S. In the eastern Pacific along 100°W, the maximum SD (more than 2.0°C) is remarkably found in the tropical North Pacific and at the depth of 50 m.

A characteristic in Figs. 2 and 3 needs to be mentioned here that the strongest signal of subsurface temperature anomalies in each month is not fixed in a specific depth. Vertically, there are many different isotherms, such as the 20°C isotherm, the 14°C isotherm, or the T_c, but it is still unknown which isotherm produces the maximum depth anomaly. It is also difficult to determine which isotherm can indicate the maximum depth anomaly in the same month and at the same tropical place. This implies that the maximum subsurface temperature anomaly in each vertical profile of the subsurface temperature anomalies in each month can be easily picked out and used to show the maximum anomalous signal in the upper ocean. Based on this consideration, two calculations from the monthly maximum subsurface temperature anomaly (MSTA) and the monthly sea surface temperature anomaly (SSTA) with respect to the monthly mean from 1980 to 1999 will be employed. The MSTA is constructed as a new index to represent the thermocline variations (Qian et al., 2003, 2004).

3. Signal propagation

The SSTA in the global ocean linearly regressed by the MSTA in Niño-3 with was analyses in our previous paper (Qian et al., 2004). The positive correlation is mainly located in the equatorial eastern Pacific and there is a very weak correlation in the central portion of the tropical Pacific basin and along the Inter-Tropical Convergence Zone (ITCZ) as well as along the South Pacific Convergence Zone (SPCZ). In order

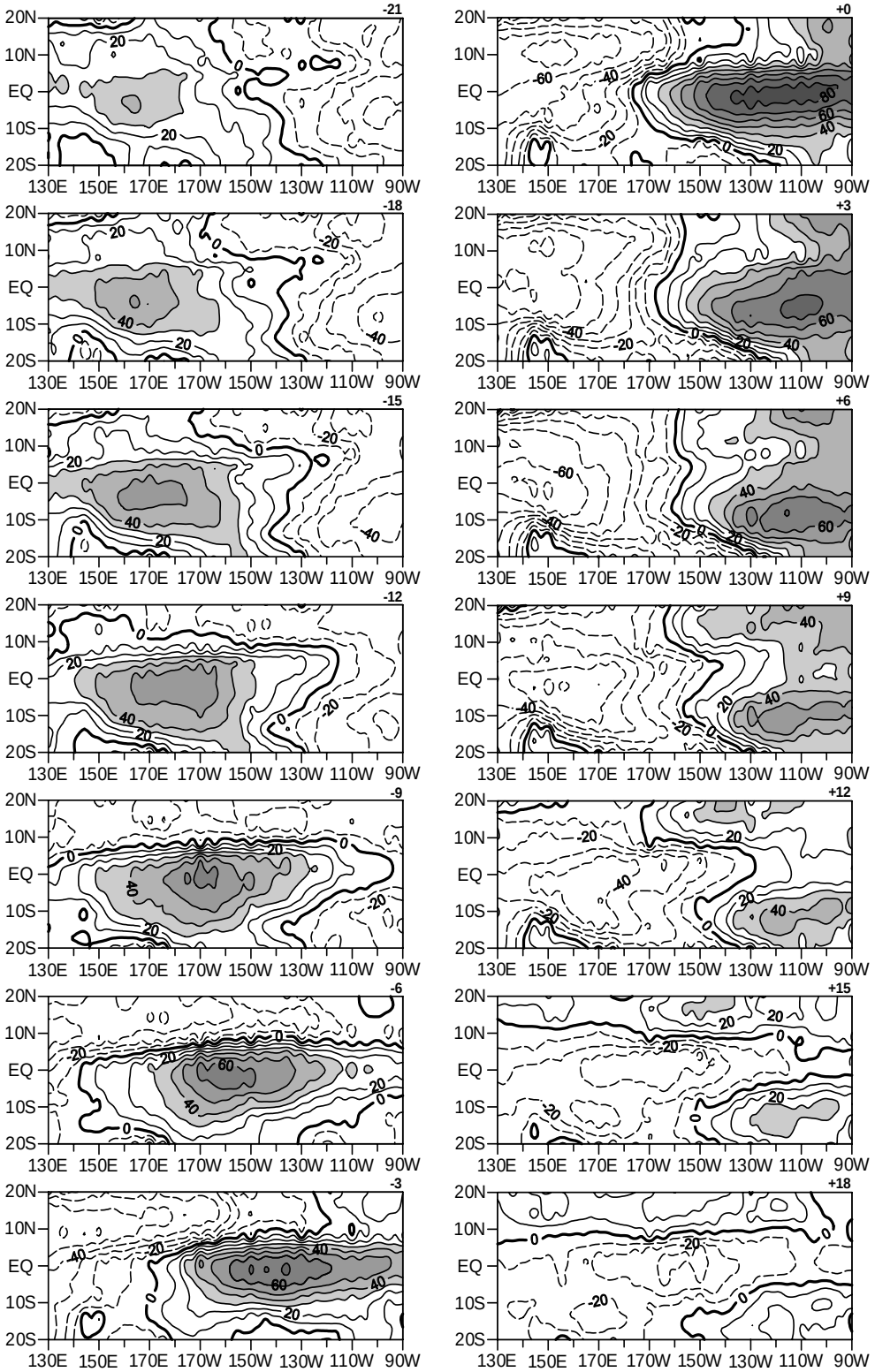

Fig. 5. Leading and lagging correlation (the values have been multiplied by 100) distributions between the Niño-3 region MSTA and the MSTA of every tropical grid based on the monthly MSTA data from 1980 to 2000. Shaded areas indicate a positive correlation larger than 0.3. The correlation coefficient 0.126 and 0.165 are the 95% and 99% levels of significance, respectively.

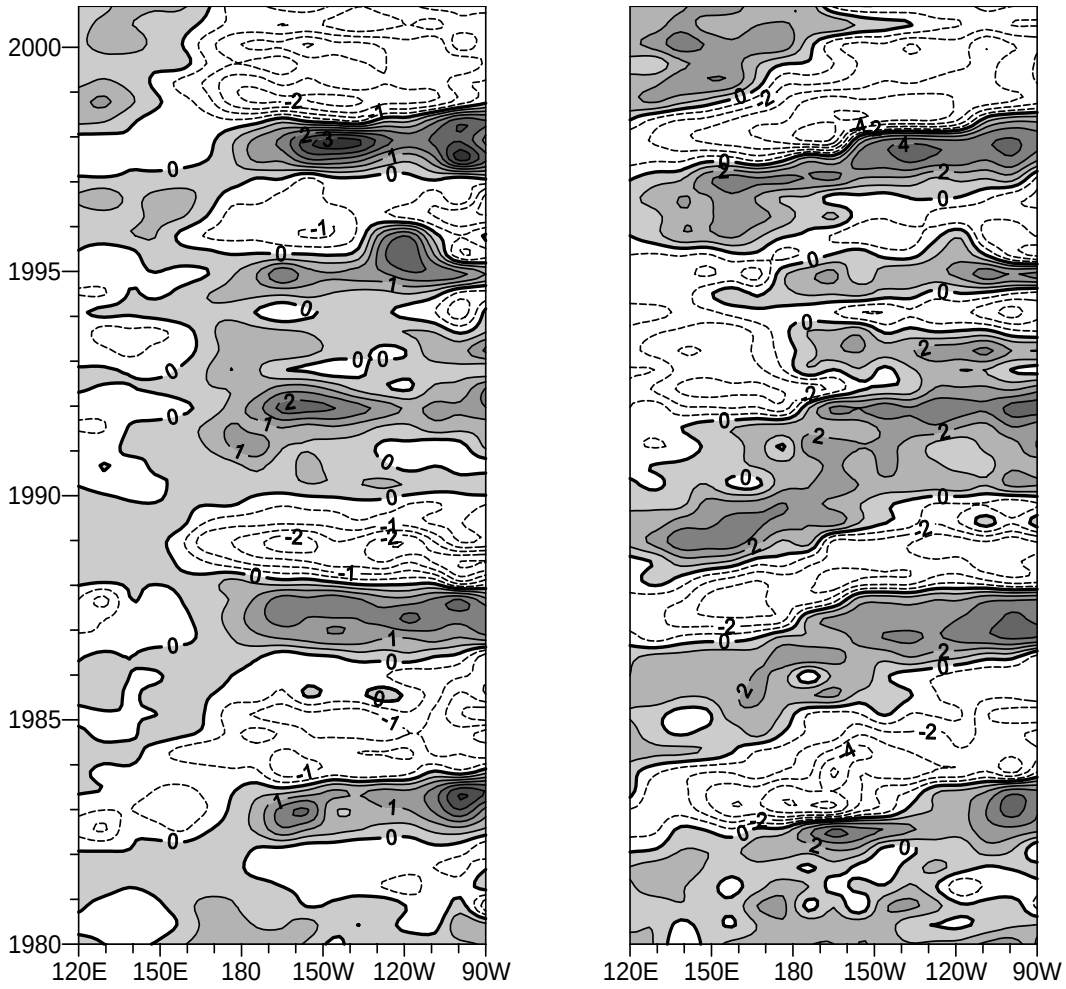

Fig. 6. Longitude-time diagrams of SSTA (left) and MSTA (right) along the equatorial Pacific. Shaded areas indicate the positive anomalies relative to the climatological mean (1980–2000). Intervals are 0.5°C for SSTA and 1.0°C for MSTA.

to further show the close relationship between the SSTA and MSTA in the Niño-3, the time series of the SSTA and MSTA in the Niño-3 region are shown in Fig. 4. Obviously, the MSTA's amplitude is larger than that of the SSTA, meanwhile the MSTA's phase is earlier than the SSTA's by about 1–2 months (the peaks of the MSTA vs those of the SSTA). The correlation coefficients of the MSTA leading the SSTA by 2, 1, and 0 months and the MSTA lagging the SSTA by 1 and 2 months are 0.82, 0.84, 0.81, 0.72, and 0.62, respectively, and all of the correlations reach 99% statistic significance. This result indicates that an El Niño (or La Niña) event mostly often occurs when a positive (or negative) MSTA propagates to the equatorial eastern Pacific. This also implies that the warming (or colding) signal in the equatorial eastern Pacific originates from the subsurface layer.

However, some questions arise as to where the MSTA signal in the eastern equatorial Pacific comes from and where it goes to. In order to answer these questions, Fig. 5 shows the leading and lagging correlation distributions between the MSTA in Niño-3 and the MSTA in the tropical Pacific Ocean from the month−21 (The MSTA in Niño-3 leads) to the month+18 (The MSTA in Niño-3 lags). The leading/lagging interval time between the any two close maps is three months. A significant signal with a correlation coefficient more than 0.3 (30 in Fig. 5) is first observed in the equatorial western Pacific since the month−21. Several other features are also noted from the evolution of this signal. Before the El Niño mature phase (in the month 0), this positive correlation center gradually moves and extends eastward along the equator (from the month−21 to the month−3 shown in Fig. 5). High correlations are limited between the ITCZ and the SPCZ during this period. At the mature

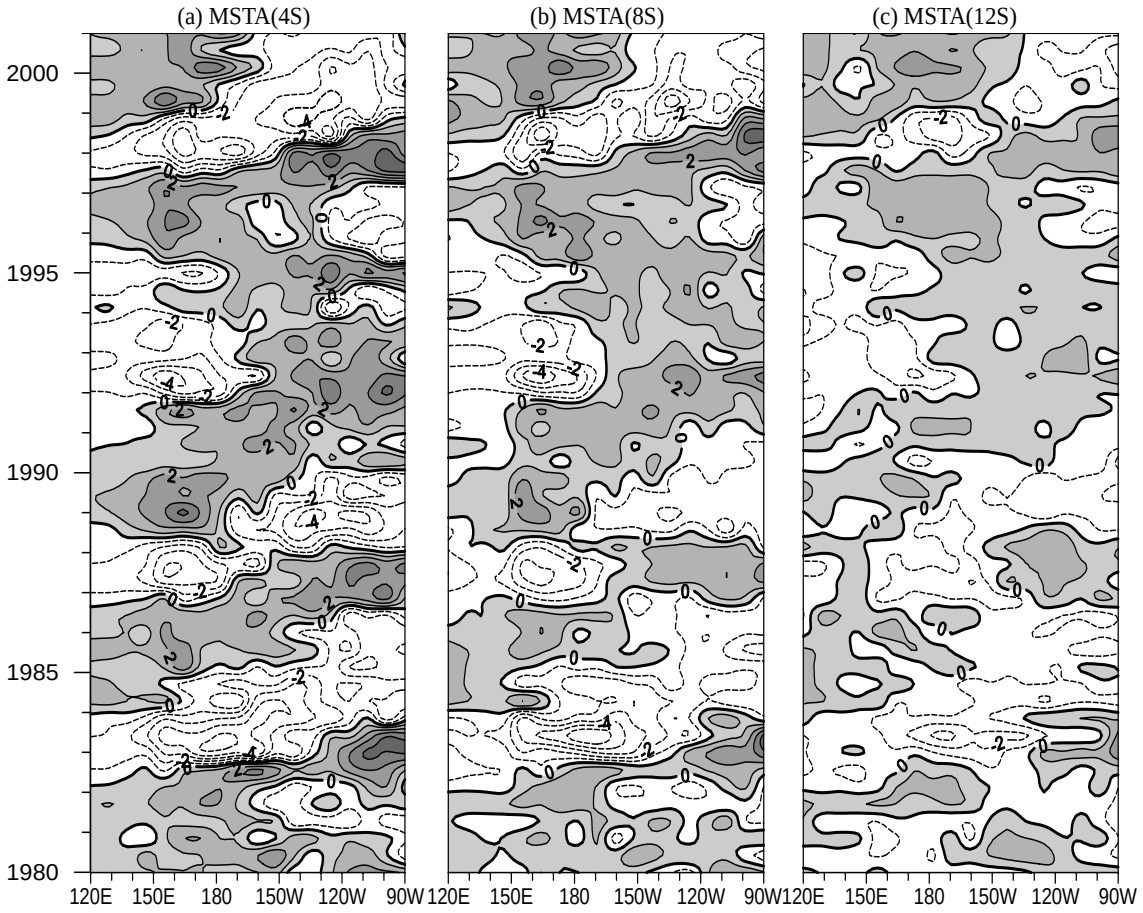

Fig. 7. Longitude-time diagrams of MSTA (°C) along the sections of 4°S, 8°S, and 12°S, respectively. Shaded areas indicate positive anomalies relative to the climatological mean (1980–2000). The interval is 1.0°C for MSTA.

phase of El Niño, the positive correlation with a value more than 0.8 (80 in Fig. 5) has been situated in the equatorial eastern Pacific, meanwhile a negative correlation with a value −0.7 (70 shown in the figure) is located in the warm pool just to the north of the equator.

After the month 0, the positive correlation coefficient center is broken into two parts. One part stands in the southeast part of the basin from the month+3 to the month+18. The other moves northward along the north side of the off-equator and then extends westward from the month+6 to the month+18. The negative correlation continue developing since the month+9 along the equator and extends eastward between the ITCZ and the SPCZ as well.

From Fig. 5, it is easy to be thought of a closed route for the warm-cold water propagation along the equator and off the equator as well as along the eastern and western boundaries of the Pacific basin. The speed of the signal across the whole basin can be estimated from Fig. 5. From the month−15 to the month−9 (within 6 months) the positive signal crosses 20° longitude, and in the following 6 months it crosses another 25°. The correlation signal propagations shown in Fig. 5 also reflect the thermocline variations which is the combination of the process of the internal oceanic dynamics with the external atmospheric forcing. Such significant change and statistical evolution regularity of the upper ocean thermal structure have important implications in the role of short-term climate variations in the ocean. By using the monthly MSTA data, propagation features of positive and negative signals along this closed route will be further examined through the analysis of single El Niño cases in the following part.

In order to compare the signal propagations based on SSTA and MSTA, Fig. 6 shows the longitude-time (month) diagrams at the equator. Along the equatorial Pacific, different propagation features can be noted

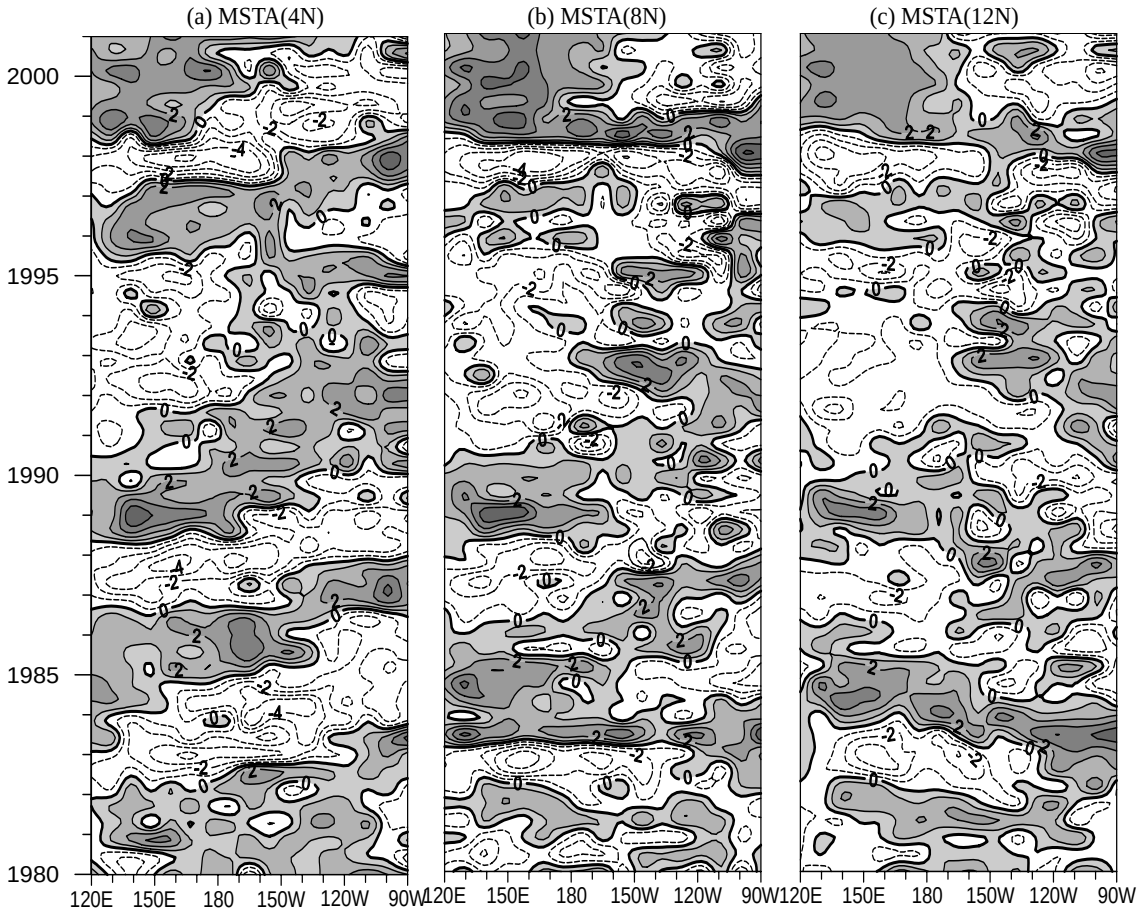

Fig. 8. Same as Fig. 7, except along the sections of 4°N, 8°N, and 12°N, respectively.

from the SSTA and the MSTA. There is no obvious propagation feature in the SSTA from 1980 to 2000, but positive-negative SSTA alternative occurrences are clear in the central-eastern Pacific. The eastward-propagation feature can be observed in the MSTA. During the period 1980–2000, five positive MSTA events in the year of 1980–81, 1985–86, 1989–90, 1994, and 1996 respectively appear in the equatorial Pacific near to the region of 150°E–170°E. Several months to one year later, these positive MSTA signals propagate to the equatorial eastern Pacific and lead to the formations of El Niño. The period of this oscillation is about 4 years, the same as the timescale of the El Niño-La Niña turnabout. From an estimation of these cases, the propagation speed eastward is about 0.46 m s^{-1}, which is still slower than the typical speed of the Kelvin wave based on the linear theory (Belamari et al., 2003).

Figures 7–9 show the propagation features of the thermocline signals in comparison with the ones in the neighbor regions, which provide a clear picture for the MSTA phase evolution involved the El Niño-La Niña turnabout.

Positive and negative signals of the thermocline variations remarkably propagate from west to east at 4°S, 8°S, and 12°S, respectively in Fig. 7. Their propagation features are consistent with the MSTA signal at the equator, but the latter is stronger than those at the off-equatorial zones. In the north side of the off-equator (shown in Fig. 8), the signal propagate eastward along 4oN and some unclear propagation along 8°N is also noted. In the year of 1980–83 and after 1995, positive and negative signals stand at 8°N. Eastward-propagating signals can be found from 1984 to 1990. Along 12°N, the signals propagate westward. However, the direction of signal propagation may be different near 10°N (figure not shown).

To the north of 12°N (Fig. 9), the MSTA signal generally propagates from east to west, but the phase speed is reduced by half at 20°N compared to that at 12°N. This speed qualities to the requirement for baroclinic Rossby waves to cross the ocean basin (Chelton and Schlax, 1996). No statistical propagation signals can be found from the SSTA (figure omitted) along 16°N, but the strongest westward-propagating signals of the MSTA can be noted along 16°N, where a high

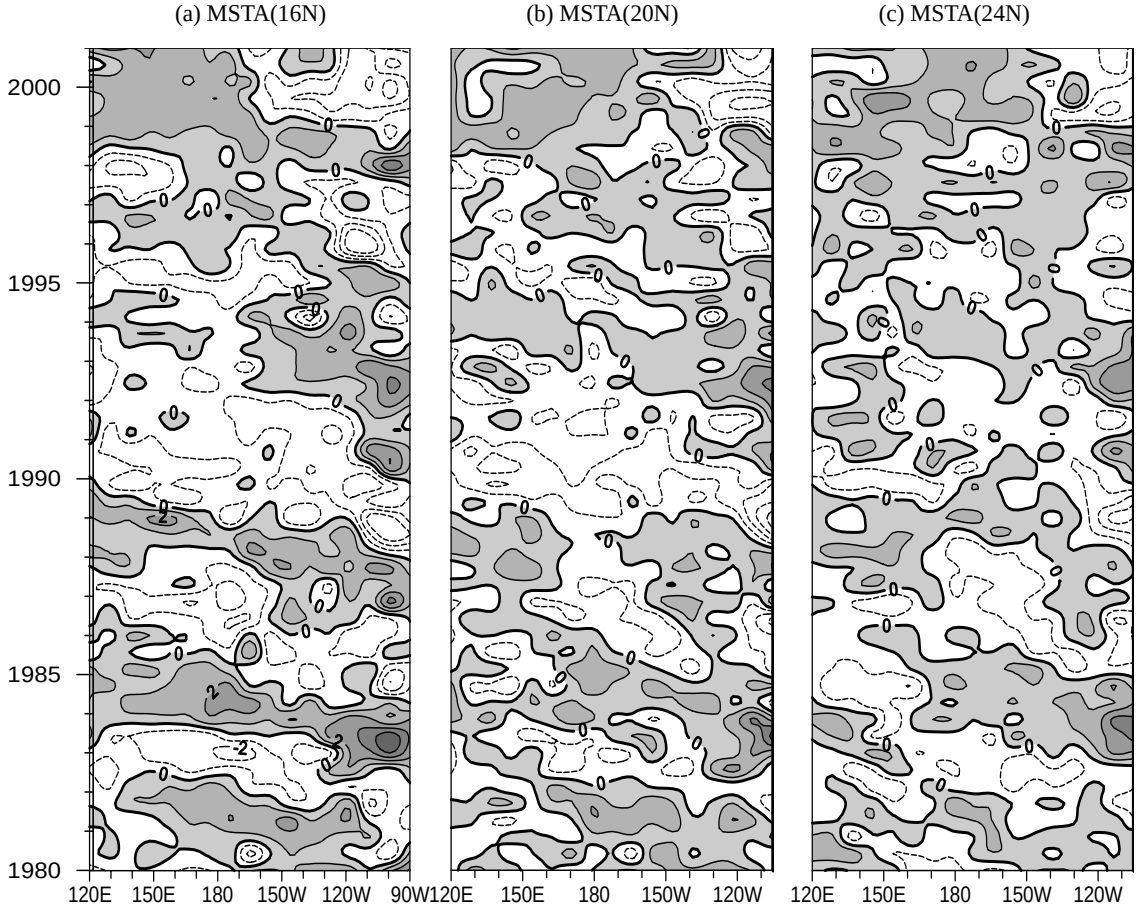

Fig. 9. Same as Fig. 7 except along the sections of 16°N, 20°N, and 24°N, respectively.

lag/lead correlation locates in Fig. 5. After the mature phase of the El Niño event in 1982/83, a positive MSTA signal is observed first in the eastern Pacific, then propagates westward, and return to the warm pool in 1984/85 (Fig. 9a). The same process can be observed in 1986/87 to 1988/89. Through the estimations of the two cases in 1984/85 and 1986/87, it takes about 2 years for the MSTA to cross the basin. This speed (about -0.4 m s^{-1}) is basically consistent with that of the baroclinic Rossby waves in the North Pacific (Chelton and Schlax, 1996).

Along 150°E (Fig. 10), the SSTAs with values from +1°C to −1°C are observed off the equator, while the MSTAs with the values from +4°C to −4°C are located just to the north of the equator. For most cases, the positive and negative MSTAs are originated from the equatorial northern Pacific near to 6°–7°N, and then propagate southward.

The El Niño-La Niña turnabout can be clearly noted from both the SSTA and MSTA at 100°W (Fig. 11) because of a shallow thermocline over there. The SSTAs with the values from +2–+3°C to −2°C can be observed near to the equator. Five El Niño processes can be clearly observed from the MSTAs along the equator. It is noted that the positive or negative MSTAs are first observed near to the equator, and then propagate slightly poleward. The MSTAs become strong again when they move back to the region of 16°N .

From these observed features, it can be identified that the positive or negative MSTAs move along a closed cycle in the northern tropics off the equator. The MSTAs first propagate from west to east along the equator, then move poleward along the eastern boundary of the basin, go back along 16°N from the eastern Pacific and arrive at the western boundary near 6°–7°N, and finally return to the equator along the western basin. From the description above, an El Niño event occurs only when a positive MSTA reaches the equatorial eastern Pacific. Rao et al (2002) showed theoretical Rossby phase speeds of about -0.48 m s^{-1} at the latitude 5°S and of about -0.16 m s^{-1} at the latitude 12°S, but no westward signal in the tropical South Pacific is observed in this study. The strongest

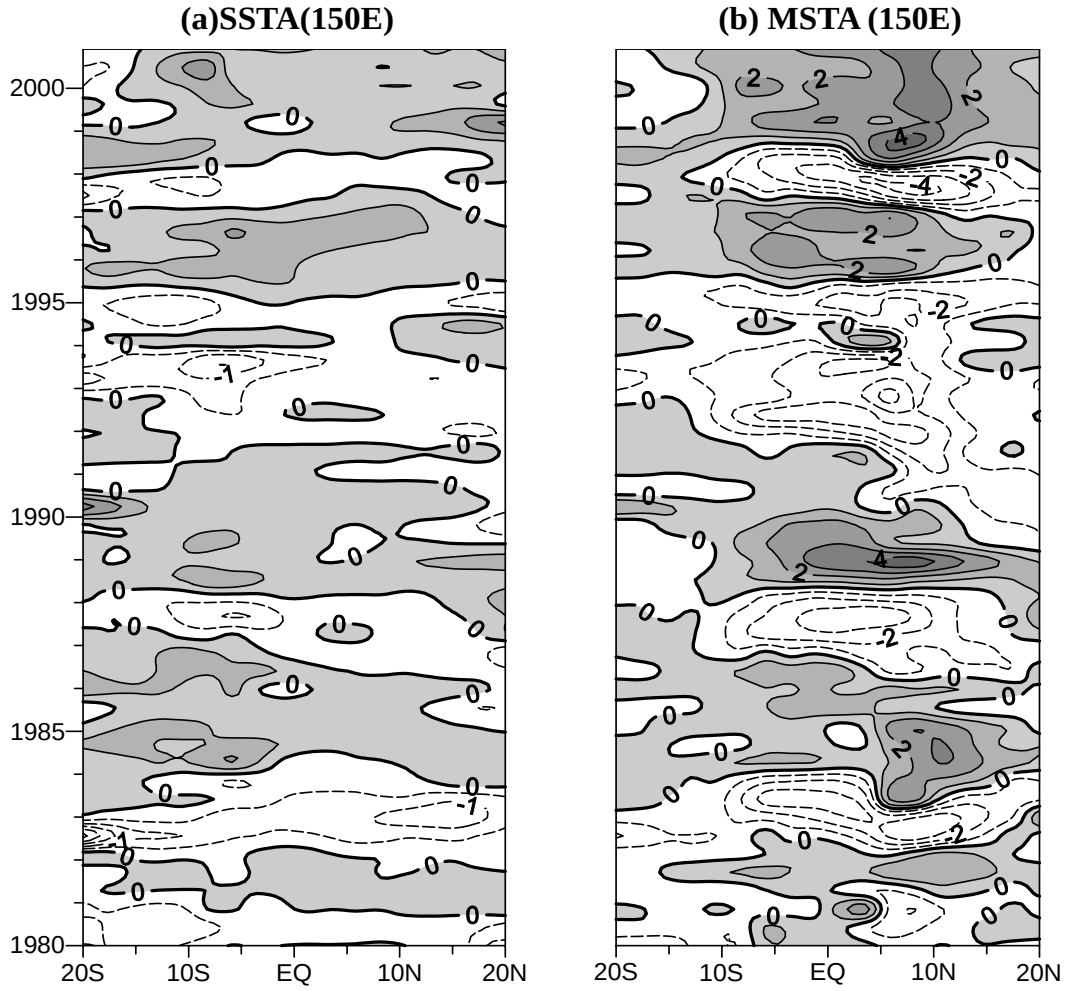

Fig. 10. Same as Fig. 6 except along the section of 150°E.

signal pathway in this closed route is only found in the tropical North Pacific.

The propagations of the subsurface temperature anomalies in the tropical Indian Ocean are also found in different zonal-time profiles. Further analyses show the intrinsic relationship of El Niño to the dipole event in the equatorial Indian Ocean. On the interannual time scale, the lower-tropospheric anomalous westerly wind first appears over the equatorial central-western Indian Ocean and then propagates eastward to the equatorial western Pacific. The anomalous westerly will cause the MSTA to propagate eastward along the equatorial Pacific. At the same time, the strong anomalous easterly over the equatorial central-eastern Indian Ocean will cause the subsurface sea temperature anomalies to propagate westward along the off-equatorial Indian Ocean. It will take about one year for a positive (or negative) MSTA signal to propagate from the west to the east along the equatorial Pacific Ocean, so the El Niño event occurs usually after about one year when the positive MSTA appears first in the tropical western Pacific. Over the equatorial central-eastern Indian Ocean, the anomalous easterly leads to the warm MSTA propagating westward along the off-equatorial Indian Ocean. It will take about half to one year for this positive MSTA signal to cross the equatorial Indian Ocean. In the Indian Ocean, the westward-propagating MSTA along the off-equator is reflected at the western boundary and then extend eastward along the equator quickly. That is why SSTA in the west is warmer than that in the east in the tropical Indian Ocean. From these analyses it can be concluded that the MSTA signal is also a precursor for predicting the dipole event in the Indian Ocean. Another two precursors have been noted that the eastward-propagating anomalous westerly over the two basins (the tropical Indian Ocean and Pacific) is the meteorological precursor to indicate the El Niño event and dipole event, while the eastward-propagating MSTA signal along the equatorial Pacific and the westward-

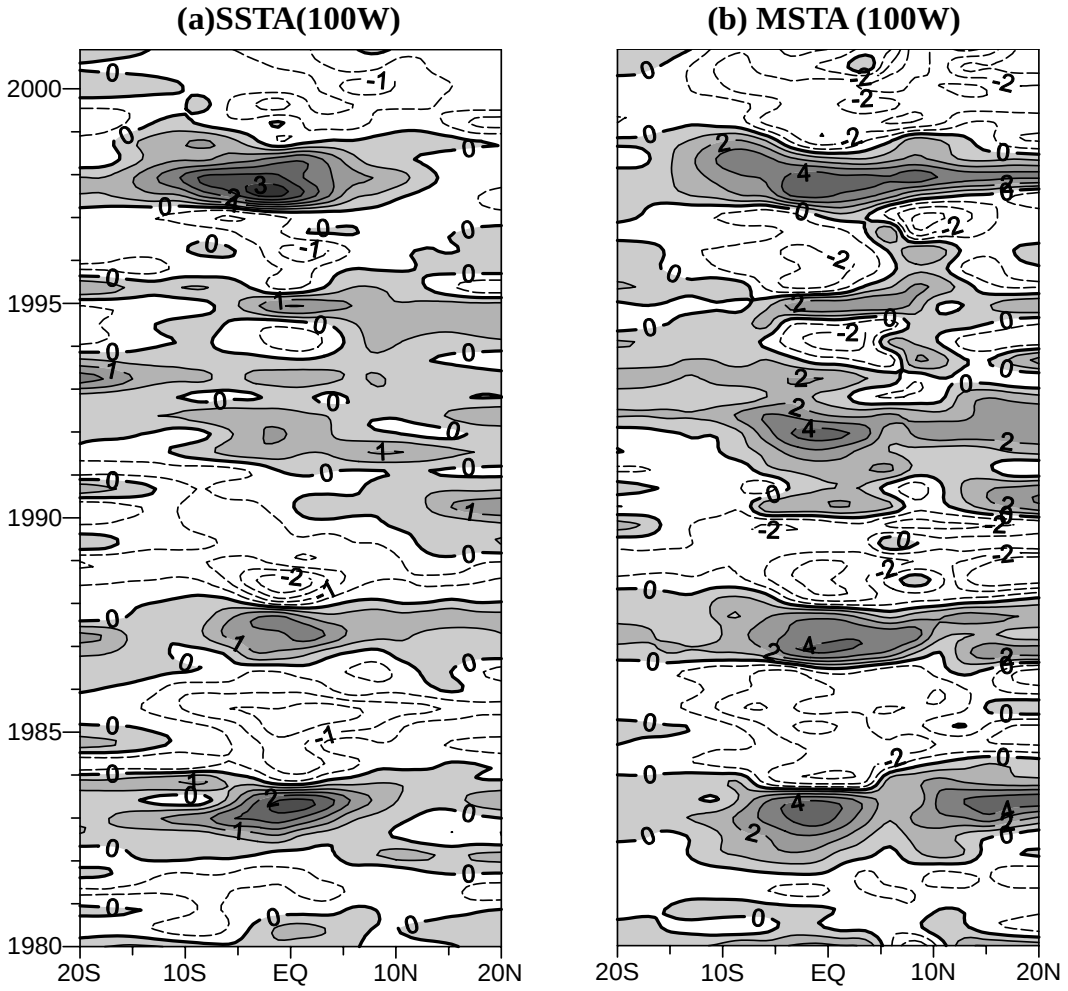

Fig. 11. Same as Fig. 6 except along the section of 100°W.

propagating MSTA signal along the off-equatorial Indian Ocean are their oceanographic precursor (Qian and Hu, 2005).

4. Comparison of MSTA and HCA

Heat content (HC) has been considered an important element for measuring the thermal status of upper oceans. Following Kinter et al. (2002), the HC is calculated as

$$\mathrm{HC} = \int_0^H T dZ/H$$

where T is the ocean temperature and $H = 400$ m is the depth of the upper ocean. To study the El Niño cycle, the annual means are removed from the HC data, and the HC anomalies (HCA) are obtained.

Three variables, SSTA, HCA and MSTA, which all reflect the oceanic state change, are used in this section. The HCA also contains some information from both the SSTA and the MSTA, but the MSTA is independent of the SSTA. In order to compare the signal propagation, Fig. 12 shows the longitude-time diagrams of both the MSTA and the HCA at the equator. From 1980 to 2000, five El Niño events with strong SSTA in the central-eastern Pacific occur in 1982–83, 1986–87, 1991–92, 1994–95 and 1997–98, respectively. The larger amplitude of the MSTA than that of the HCA can be noted across the Pacific basin. During the whole period of 1980–2000, five positive MSTA and HCA events appeared in 1980–81, 1985–86, 1989–90, 1994 and 1996 originally in the equatorial western Pacific (EWP) near to 150°–170°E. After several months to one year these positive MSTA signals propagate to the equatorial eastern Pacific (EEP) and lead to the outbreak of El Niño. Through their comparison, it is also found that the standing oscillation in the SSTA signal can be observed in the central-eastern Pacific (Fig. 6), while the mobile oscillations are noted in the MSTA and HCA (Fig. 12). Comparatively, MSTA sig-

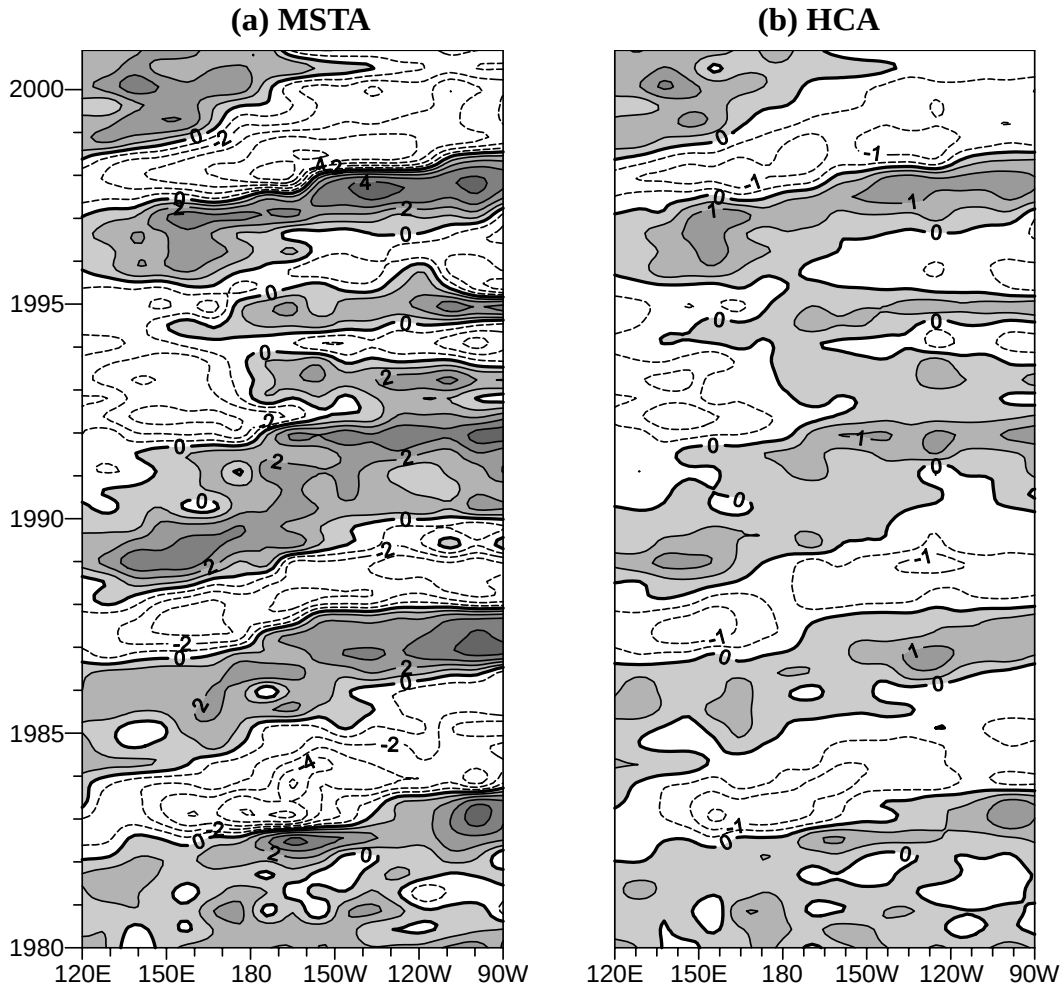

Fig. 12. Longitude-time diagrams of (a) MSTA and (b) HCA along the equatorial Pacific. Shaded areas indicate the positive anomalies and the intervals are 1°C for MSTA while 0.5°C for HCA.

nals are more obvious than those of the HCA.

The standard deviations of SSTA, MSTA and HCA as well as their correlations in the tropical Pacific are calculated and shown in Fig. 13. For the SSTA (Fig. 13a), the most outstanding feature is the well-defined pattern of high standard deviation with values larger than 1.0°C in the equatorial central-eastern Pacific, while the low correlation is located in its two sides off the equator. This feature is similar to the surface warming at the mature phase of El Niño. For the HCA (Fig. 13b), two major centers of the standard deviation with values larger than 0.8°C are located near to the southern Philippine Sea in the northern region and the Solomon Islands (east of New Guinea) in the southern region, respectively. Moderately high standard deviation also appears along the equator in the central-eastern Pacific. Thus, the high standard deviations of both the HCA and the SSTA coexist in the equatorial central-eastern Pacific. However, along the ITCZ and the SPCZ, the low standard deviation of the SSTA coexists with the high standard deviation of the HCA. The above features indicate that while SST has its largest standard deviation in the eastern Pacific, the strong variability of the subsurface temperature with two separate centers off the equator locates in the western Pacific. Lysne and Deser (2002) analyzed the spatial patterns of the interannual temperature variation at two representative depths (200 and 400 meters), and pointed out that these distributions of thermal variation are coincident with the maximum variance of wind stress curl in the tropical western Pacific.

The SD pattern of the MSTA is different from that of the SSTA and the HCA in the tropical Pacific Basin (Fig. 13c). The large MSTA SD (more than 2°C) appears in the tropical basin between 8°S and 12°N with

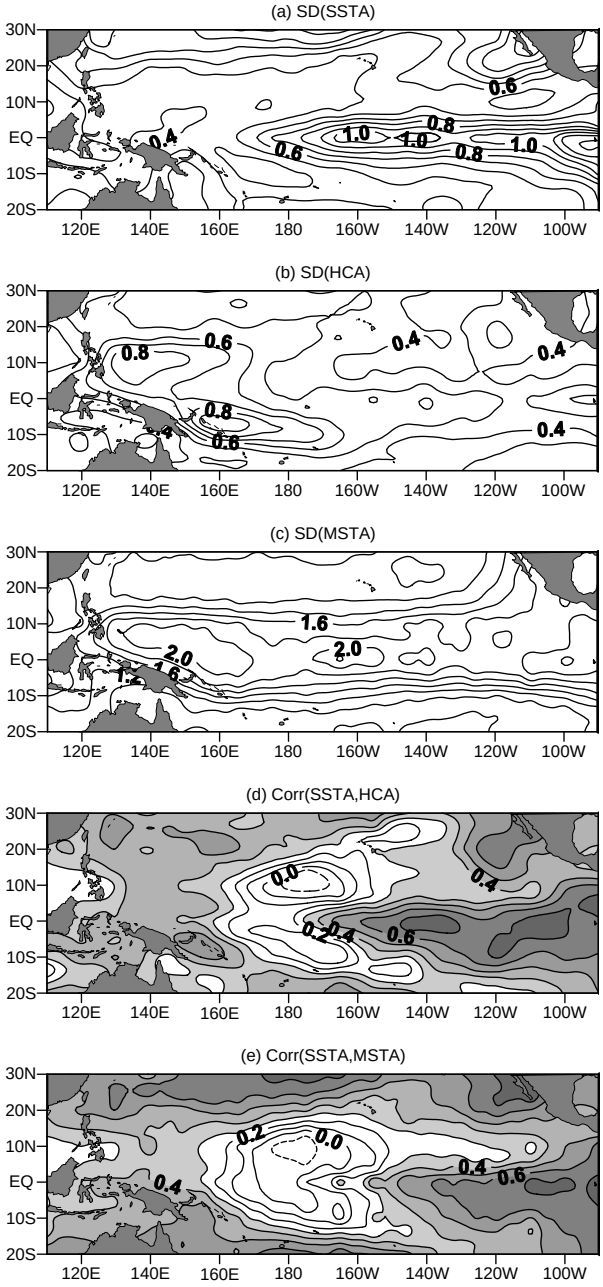

Fig. 13. Standard deviations (°C) of (a) SSTA (b) HCA and (c) MSTA as well as correlations (d) between HCA and SSTA, and (e) between MSTA and SSTA. The shaded are the values larger than 0.6°C in (a), (b) and (c), and those significant at the 95% confidence level in (d) and (e).

several centers larger than 2.0°C scattering in the western, central and eastern portion of the basin. The largest SD of the MSTA is also located in the equatorial central-eastern Pacific. This result shows that the largest SD generally exists in the SSTA, MSTA and HCA in the EEP.

As seen in Fig. 13d, the correlation between the SSTA and the HCA displays a major high-value band in the equatorial eastern Pacific. In particular, the correlation coefficient exceeds 0.7 in the part of the Niño-3 region. Local high correlations also appear in the western Pacific in both hemispheres. On the other hand, the butterfly-shaded low correlation is observed in the central Pacific. The low correlation implies that the subsurface signal in the HCA cannot be reflected from the SSTA in the central Pacific. This butterfly-shaded low correlation is also observed in the correlation pattern between the SSTA and the MSTA (Fig. 13e).

Through these analyses, it is noted that the larger SD and higher correlation are observed in the EEP region (the Niño-3 region). Figure 14 shows the monthly variations of the SSTA and HCA in the Niño-3 region. Both the SSTA and HCA exhibit a similar interannual variability. The simultaneous correlation between the two time series is 0.86 but the lagging relationship is clearer between the SSTA and the MSTA than between SSTA and HCA.

It is found that the HCA signal also propagates along the equator and a high correlation is in the Niño-3 region. Figure 15 shows the patterns of lead-lag correlation between the Niño-3 HCA and the HCA in the tropical Pacific. In the 21 months earlier than the peak of the Niño-3 HCA (Fig. 15a), a center of positive correlation appears in the equatorial western Pacific, which indicates a possible precursory signal for the Niño-3 HCA. At the time when the Niñ-3 HCA lags 18 to 6 month, the positive correlation center intensifies and moves eastward along the equator. The signal propagation with the strongest signal pathway along the equator is highly limited between the Intertropical Convergence Zone and the South Pacific Convergence Zone. At the zero lag (Fig. 15e), the correlation pattern is similar to the SSTA at the mature phase of El Niño, suggesting again a close relationship between the HCA and the SSTA in the equatorial eastern Pacific. Note that afterwards the positive center is split off the equator and moves westward along the off-equator zones (Figs. 15f–h). This feature is similar to the MSTA.

5. Conclusion and discussion

A summary about the indicators and precursors in the thermocline variations in the tropical Pacific basin is made in this section. Table 1 summarizes traveling signals in the tropical Pacific under the different definitions of the thermocline variations and in different timescales. According to Meyers' (1979) definition, the

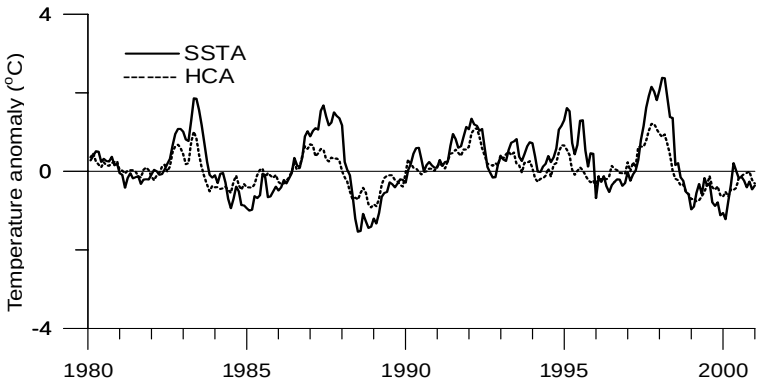

Fig. 14. Time series of the monthly SSTA (°C) and HCA (°C) in the Niño-3 region (5°N–5°S, 150°–90°W).

Table 1. Traveling signals in the tropical Pacific under the different indexes and various timescales.

Authors	Index	Eastward signal band	Westward signal	Timescale
Meyers (1979)	14°C isotherm depth		Along 6°N	Annual
Kessler (1990)	20°C isotherm depth		Around 10°N	Annual
Wang et al. (2000)	Location-dependent T_c depth	2°S–2°N	5°N and 6°S	Annual
Chao et al. (2002)	Curved surface (STA)	Along the equator	10°N and 10°S	Interannual
Chelton and Schlax (1996)	Satellite altimeter	2°S–2°N	4°N and 4°S	Intraseasonal
This paper	MSTA	10°S–10°N	16°N	Interannual

14°C isotherm depth variations, reveals the westward-propagating annual signal along the latitude 6°N. In Kessler's (1990) definition, the 20°C isotherm depth variations, explores the westward-propagating annual signal around the latitude 10°N. Wang et al. (2000) defined a location-dependent subsurface temperature and found the eastward-traveling signal along the equatorial band 2°S–2°N and the westward-traveling signals along 5°N and 6°S on the annual timescale. Chao et al. (2002) defined a temperature curved surface and found the anomalous signal traveling eastward within 2° of the equator and traveling westward along 10°N and 10°S, respectively, on the interannual timescale. By using satellite altimeter data, Chelton and Schlax (1996) found an eastward traveling signal within 2° of the equator and westward traveling signals along 4°N and 4°S on the intraseasonal timescale. Under these papers's definitions, an eastward-traveling signal is all found in the band 10°S–10°N and a westward-traveling signal is also found and centered along the latitude 16°N. Through comparing the HCA with the MSTA, it is noted that both have similar travel feature, but the amplitude and phase of the SSTA is much localized.

Based on the composite analysis of El Niño events, a new index from the maximum subsurface temperature anomaly (MSTA), representing the vertical temperature profile, is proposed to display the thermocline variation in the tropical Pacific Basin. The significant correlation between the MSTA and the SSTA is situated in the equatorial eastern Pacific so that the MSTA instead of the SSTA in the eastern equatorial Pacific may be used to find out possible early signals for El Niño. In the equatorial eastern Pacific, the MSTA signal is earlier than the SSTA by about 2 months. This means that the vertical advection of the MSTA is important for the formation of El Niño in the eastern equatorial Pacific.

The propagating MSTA signal is robust in the tropical North Pacific with an anti-clockwise cycle along the equator and the region just to the north of the equator. The eastward and westward propagations of the MSTA signals are separated around 10°N. An MSTA signal propagates eastward along the equator in a way like the Kelvin wave, but its propagation is slower than the phase speed of the theoretical Kelvin wave and the signal needs more than one year to travel across the Pacific basin. The signal propagates poleward along the eastern boundary in the coastal Kelvin-like wave. Off the north side of the equator, the positive (negative) MSTA propagates westward with the strongest signal near to 16°N from the eastern boundary to the western boundary near to the band 6°–7°N in the Rossby-like wave; its speed is consistent with the phase speed of the theoretical Rossby wave.

The propagations of the subsurface signals in the

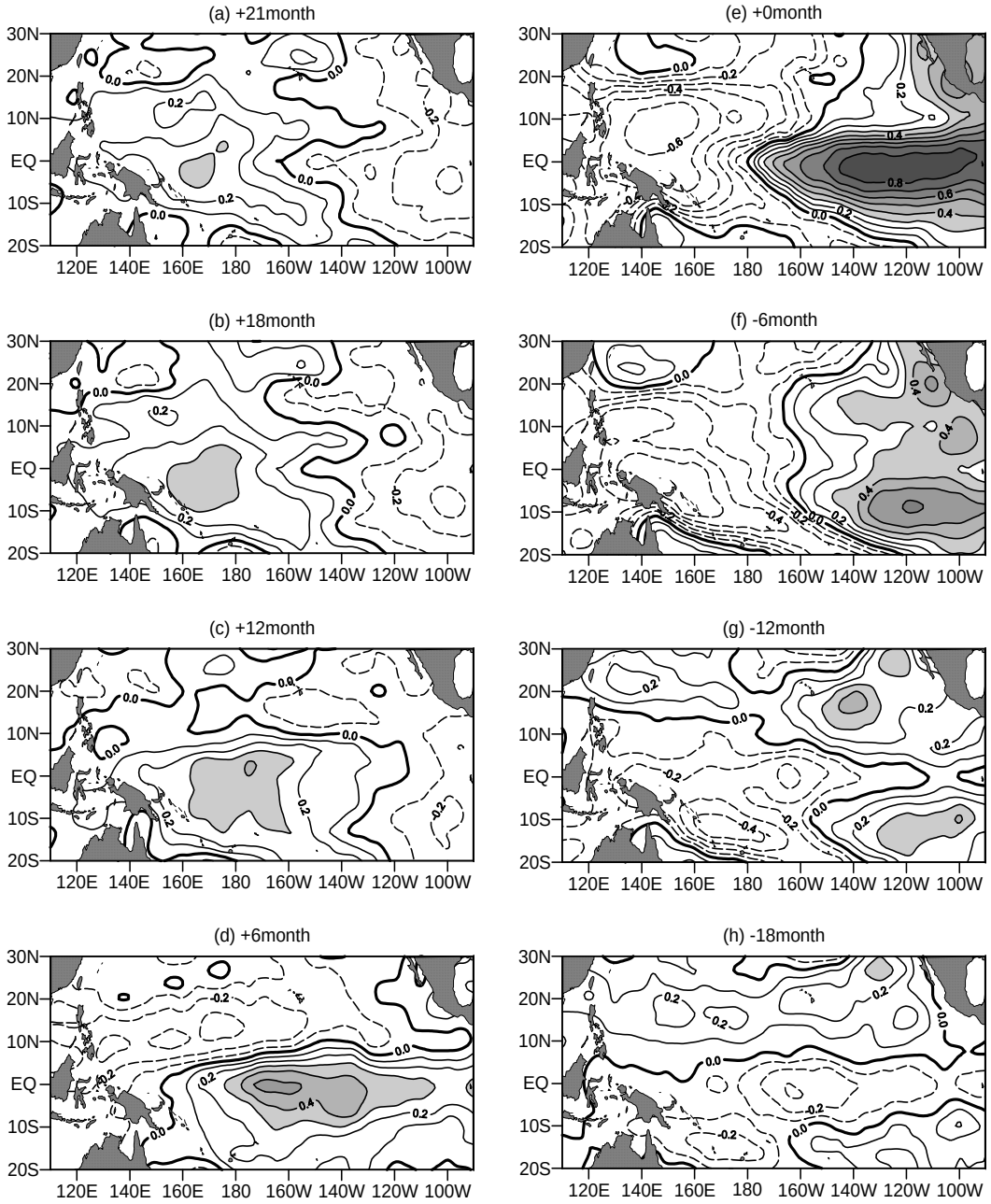

Fig. 15. Leading and lagging correlations between Niño-3 HCA and the HCA at each grid point. In (a), "+21" denotes that the grid-point HCA leads the Niño-3 HCA by 21 months. Values larger than the 95% confidence level are shaded. The contour interval is 1.

tropical Pacific basin are involved in some advection processes as indicated by Belamari et al. (2003), such as vertical advection, zonal advection, and meridional advection. Among these advections, the vertical and zonal advections are two important processes. In the central Pacific, the zonal advection is dominant over others, while in the equatorial eastern Pacific basin, the vertical advection is crucial in the process of the El Niño development.

The MSTA, as an indicator of thermocline variations, is a better index than the others because it captures the strongest signal in the upper ocean. The MSTA signal may actually be a dynamical signal in the upper ocean. An anomalous signal indicated by satellite altimeters may reflect the intraseasonal impact from the coupled atmospheric-ocean sys-

tem rather than only free propagating waves below the surface. Different pathways of the signal propagation from other definitions may be associated with different timescales and different depths of oceanic variations because these waves are strongly influenced by various oceanic depths.

Although the signal propagation of the MSTA at the equator across the basin is analyzed, however, the speed is considerably smaller than that of the theoretical equatorial Kelvin wave. The reason for this may be linked to the air-sea interaction in the tropical Pacific, which should be investigated in more detail in the future.

Acknowledgments. We thank the two reviewers for helpful comments and suggestions that improved the manuscript. This research was supported by the National Basic Research Program of China (Grant No. 2006CB403602).

REFERENCES

Belamari, S., J. L. Redelsperger, and M. Pontaud, 2003: Dynamic role of a westerly wind burst in triggering an equatorial Pacific warm event. *J. Climate*, **16**(12), 1869–1890.

Boulanger, J. P., and C. G. Menkes, 1995: Propagation and reflection of long equatorial waves in the Pacific Ocean during the 1992–1993 El Niño. *J. Geophys. Res.*, **100**, 25041–25059.

Chao Jiping, Yuan Shaoyu, Chao Qingchen, and Tian Jinei, 2002: A data analysis study on the evolution of the El Niño/La Niña cycle. *Adv. Atmos. Sci.*, **19**(5), 837–843.

Chelton, D. B., and M. C. Schlax, 1996: Global observations of oceanic Rossby waves. *Science*, **272**(12), 234–238.

Kessler, W. S., 1990: Observations of long Rossby waves in the northern tropical Pacific. *J. Geophys. Res.*, **95**, 5183–5217.

Kinter, J. L., K. Miyakoda, and S. Yang, 2002: Recent change in the connection from the Asian monsoon to ENSO. *J. Climate*, **15**(10), 1203–1215.

Li, T., 1997: Phase transition of the El Niño-Southern Oscillation: A stationary SST mode. *J. Atmos. Sci.*, **54**, 2872–2887.

Li Chongyin, 2002: A further study of essence of the ENSO. *Climatic and Environment Research*, **7**(2), 160–174. (in Chinese)

Li Congyin, and Mu Mingquan, 1999: El Niño occurrence and sub-surface ocean temperature anomalies in the Pacific warm pool. *Chinese J. Atmos. Sci.*, **23**(5), 513–521.

Lysne, J., and C. Deser, 2002: Wind-driven thermocline variability in the Pacific: A model-data comparison. *J. Climate*, **15**, 829–845.

Meyers, G., 1979: On the annual Rossby wave in the tropical North Pacific Ocean. *J. Phys. Oceanogr.*, **9**, 663–674.

Qian Weihong, and Hu Haoran, 2005: Signal propagation and linkages of subsurface temperature anomalies in the tropical Pacific and Indian Ocean. *Progress in Natural Science*, **15**(5), 579–584.

Qian Weihong, Zhu Yafen, and Ye Qian, 1999: Interannual and interdecadal variability in SST anomaly over the eastern equatorial Pacific. *Chinese Science Bulletin*, **44**(6), 568–571.

Qian, W. H., Hu, H. R., and Zhu, Y. F., 2003: Thermocline oscillation and warming event in the tropical Indian Ocean. *Atmos.-Ocean*, **40**(3), 241–258.

Qian, W. H., Y. Zhu, and J. Liang, 2004: Potential contribution of maximum subsurface temperature anomalies to the climate variability. *International Journal of Climatology*, **24**, 193–212.

Rao, S. A., S. K. Behera, and Y. Masumoto, 2002: Interannual subsurface variability in the Tropical Indian Ocean with a special emphasis on the Indian Ocean dipole. *Eastern Equatorial Pacific-Sea Research II*, **49**, 1549–1572.

Rasmusson, E. M., and T. H. Carpenter, 1982: Variations in tropical sea surface temperature and surface wind field associated with the Southern Oscillation/El Niño. *Mon. Wea. Rev.*, **110**, 354–384.

Wang, B., 1995: Interdecadal changes in El Niño onset in the last four decades. *J. Climate*, **8**, 267–285.

Wang, B., R. C. Wu, and R. Lukas, 2000: Annual adjustment of the thermocline in the tropical Pacific Ocean. *J. Climate*, **13**, 596–616.

White, W. B., 1995: Design of a global observing system for gyre-scale upper ocean temperature variability. *Progress in Oceanography*, **36**, 169–217.

Yang, Y. J., T. Y. Tang, and R. H. Weisberg, 1997: Basin-wide zonal wind stress and ocean thermal variations in the equatorial Pacific Ocean. *J. Geophy. Res.*, **102**(C1), 911–927.

Yu, W. D., and F. L. Qiao, 2003: Analysis of the Heat Content Variability of the Tropical Pacific Upper Ocean During ENSO Events. *Advances in Marine Science*, **21**(4), 446–453. (in Chinese)

Zebiak, S. E., and M. A. Cane, 1987: A model El Niño-Southern Oscillation. *Mon. Wea. Rev.*, **115**, 2262–2278.